International Journal of Nanomedicine

Dovepress
open access to scientific and medical research

Open Access Full Text Article

ORIGINAL RESEARCH

Alginate Hydrogels with Embedded ZnO Nanoparticles for Wound Healing Therapy

This article was published in the following Dove Press journal:
International Journal of Nanomedicine

Carol M Cleetus[1]
Fabian Alvarez Primo[1]
Gisel Fregoso[2]
Nivedita Lalitha Raveendran[3]
Juan C Noveron[4]
Charles T Spencer[5]
Chinatalapalle V Ramana[3]
Binata Joddar[1]

[1]Department of Metallurgical, Materials and Biomedical Engineering, The University of Texas at El Paso, El Paso, TX 79968, USA; [2]Department of Electrical and Computer Engineering, The University of Texas at El Paso, El Paso, TX 79968, USA; [3]Department of Mechanical Engineering, The University of Texas at El Paso, El Paso, TX 79968, USA; [4]Department of Chemistry and Biochemistry, The University of Texas at El Paso, El Paso, TX 79968, USA; [5]Department of Biological Sciences, The University of Texas at El Paso, El Paso, TX 79968, USA

Introduction: In this in-vitro study, we designed a 3D printed composite of zinc oxide (ZnO) nanoparticles (NPs) with photocatalytic activities encapsulated within hydrogel (alginate) constructs, for antibacterial purposes applicable towards wound healing. We primarily sought to confirm the mechanical properties and cell compatibility of these ZnO NP infused scaffolds.

Methods: The antibacterial property of the ZnO NPs was confirmed by hydroxyl radical generation using ultraviolet (U.V.) photocatalysis. Titanium dioxide (TiO_2), a well-known antibacterial compound, was used as a positive control (1% w/v) for the ZnO NP-based alginate constructs and their antibacterial efficacies compared. Among the ZnO group, 3D printed gels containing 0.5% and 1% w/v of ZnO were analyzed and compared with manually casted samples via SEM, swelling evaluation, and rheological analysis. Envisioning an in-vivo application for the 3D printed ZnO NP-based alginates, we studied their antibacterial properties by bacterial broth testing, cytocompatibility via live/dead assay, and moisture retention capabilities utilizing a humidity sensor.

Results: 3D printed constructs revealed significantly greater pore sizes and enhanced structural stability compared to manually casted samples. For all samples, the addition of ZnO or TiO_2 resulted in significantly stiffer gels in comparison with the alginate control. Bacterial resistance testing on *Staphylococcus epidermidis* indicated the addition of ZnO NPs to the gels decreased bacterial growth when compared to the alginate only gels. Cell viability of STO-fibroblasts was not adversely affected by the addition of ZnO NPs to the alginate gels. Furthermore, the addition of increasing doses of ZnO NPs to the alginate demonstrated increased humidity retention in gels.

Discussion: The customization of 3D printed alginates containing antibacterial ZnO NPs leads to an alternative that allows accessible mobility of molecular exchange required for improving chronic wound healing. This scaffold can provide a cost-effective and durable antibacterial treatment option.

Keywords: zinc oxide nanoparticles, chronic wound healing, 3D printing, antibacterial, hydroxyl radicals, alginate hydrogels/scaffolds

Introduction

The early treatment and rapid closure are essential for the healing of chronic wounds for the prevention of hypertrophic scarring.[1] In the United States alone, chronic wounds, including diabetic foot ulcers, affect up to 6 million patients amounting to $10 billion each year.[2] The treatment and care of such non-healing chronic wounds that do not respond well to conventional wound-healing strategies affect not only the patient and the society, but the resulting morbidity and cost are considerable. Therefore, the establishment of novel approaches for the treatment of

Correspondence: Binata Joddar
Email bjoddar@utep.edu

submit your manuscript | www.dovepress.com
DovePress
http://doi.org/10.2147/IJN.S255937

chronic wounds is much needed. Commercially available advanced skin substitutes, comprising of bioactive dressings containing mammalian derived matrix components, and human cells, have widespread clinical applications.[3] The use of autografts is often limited by the availability of a suitable area of healthy donor skin to harvest. Alternative treatment options for these patients include the application of cellular and non-cellular biological skin-equivalents.[4] However, these treatments involve multiple surgical procedures and are associated with high costs of production and repeated wound treatment.[4] Despite all these existing strategies for the treatment of non-healing chronic wounds, it is presently accepted that no treatment significantly outperforms the others.[5] There are a few emerging options, including "smart" peptide hydrogels for first-line treatment in burn wounds.[6] Self-assembling peptides have tunable properties making them popular in various applications.[7] However, not enough consideration has been attributed to understanding the interfacial dynamics between the wound healing template and the wound zone. To address this unmet challenge, we focused on developing an innovative 3D printed, acellular scaffold composed of alginate hydrogels, impregnated with ZnO NPs as a more efficacious wound healing therapy, compared to existing products.

Biopolymers such as alginic acid (alginate) have gained recognition in various applications. One such instance is their use in packaging pharmaceuticals or drug delivery systems. Other uses of packaging polymers are found in the food sector.[8] Alginate based hydrogels are being researched for environmental applications, as well, for their hydrophilic, swellable, and modifiable characteristics.[9] Alginate is a natural material derived from carbohydrate sources released by clinical bacterial species, in the same manner as biofilm formation. These polymers are well utilized over others in medicine due to their biocompatibility, biodegradability, and accessibility.[10] Alginate retains up to 70% water by volume. Therefore, these types of dressings are best used on wounds that have a large amount of exudate as the hydrogel can absorb the exudate secreted from the wound, thereby reducing its bioburden.[11] As calcium alginate is a natural hemostat, alginate-based dressings, which act as inherent tissue sealants, are designated for the treatment of non-healing chronic wounds. The gel-forming property of alginate helps form an effective seal against fluid leakage leading to bonding between adjacent tissue surfaces that further helps in painless debridement and alleviates the pain experienced by the patient during dressing changes.[11–13] It also provides a moist environment that leads to rapid granulation and re-epithelialization of the wound area leading to the healing of split skin graft at the donor site.[13] As a result, alginate-based wound dressings are well established in the literature and in clinical wound management.[14] Based on this knowledge, we hypothesized that this alginate biomaterial-based wound healing template could be precisely engineered by 3D bioprinting leading to effective nutrient and water exchange required for improving chronic wound healing.

However, there is no evidence of superior effectiveness of alginate-based wound dressings in those with diabetic foot ulcers, which is an outstanding example of non-healing chronic wounds. Diabetic wounds lack their innate ability to heal and require immense support from the wound healing templates used, to promote normal healing and tissue growth. This is complexed by the deficiency of the cells in this wound region that do not secrete growth factors such as platelet-derived growth factor (PDGF), vascular endothelial growth factor (VEGF), and transforming growth factor-beta (TGF-β), required for normal wound healing.[15] Studies from other groups have shown that these cells do not respond to growth factors even when they are delivered externally from the template during the tissue healing process, as these factors need to be released at specific periods, internally within the wound.[16] Therefore, we conceived the idea of adding zinc oxide (ZnO) to an alginate-based template, as the micronutrient Zn present in ZnO is known to promote angiogenesis (de-novo blood vessel formation) thereby leading to tissue healing and recovery.[17] The dissolution of ZnO particles releases Zn^{2+} ions in aqueous suspension that adds to the antimicrobial activity of ZnO.[18] ZnO NPs, when combined with alginate, also enhance the mechanical properties possessed by these and other natural polymers.[19] In addition, ZnO NPs can generate reactive oxygen species allowing for an additional mechanism to combat the recent increases in antibacterial resistance due to antibiotic treatment options.[10,19]

Therefore, in this study, we applied in-house synthesized ZnO NPs, which naturally possess antibacterial properties and are additionally photocatalytic in the ultraviolet (UV-B) light range, enabling them to release powerful hydroxyl (-OH) free radicals for the termination of harmful pathogens and bacteria in the wound site.[20] This further led to the idea of a 3D printed customized wound-healing template consisting of ZnO NPs homogeneously dispersed within an alginate template that can be designed readily

and made to fit the exact size and depth of the wound using contour printing.[21] 3D printing is a layer by layer addition of material allowing for the creation of unique shapes and offering the customizability important biomedical sectors tissue engineering or pharmaceutics. Several different techniques can be employed in 3D printing.[22] Extrusion 3D printing was adopted for the development of such a uniquely designed wound healing template. The addition of ZnO NPs to the alginate pre-gel solution was expected to enhance its shear-thinning properties as well as printability and extrusion from a 3D bioprinter.[23] The resultant calcium ion cross-linked gel-like structure is highly hydrophilic and helps form a slow degradable cross-linked polymer gel, which will limit wound secretions and minimize bacterial contamination. 3D printed templates were expected to confer additional structural fidelity and a slower rate of degradation followed by sustained retention of moisture, compared to manually casted gel templates. Since the alginate scaffold is completely biodegradable in-vivo, this phenomenon makes this particular concept more patient-friendly and marketable. Although ZnO is a potent antibacterial, its concentration in wound healing therapies need to be optimized, as higher amounts can be toxic in-vivo. Therefore, we designed this study to include several doses of ZnO mixed within 3D printed alginate gels to optimize their printability, antibacterial properties, and biocompatibility.

Materials and Methods

Materials Used

The principal chemicals and reagents used in this study, Sucrose ($C_{12}H_{22}O_{11}$) and Zinc Nitrate Hexahydrate ($Zn(NO_3)_2$•$6H_2O$) for the synthesis of ZnO NPs were purchased from Sigma-Aldrich Inc (St. Louis, MO). Medium Viscosity Alginic Acid Sodium Salt (($C_6H_7O_7$)A($C_6H_7O_7$)BNa) (alginate), Calcium Chloride Dihydrate ($CaCl_2$•$2H_2O$), Phosphate Buffered Saline (PBS,10X), Sodium Hydroxide (NaOH) and Terephthalic Acid ($C_8H_6O_4$) were all obtained from Thermofisher Scientific (Waltham, MA).

Synthesis and Characterization of ZnO NPs

In this study, zinc oxide nanoparticles (ZnO NPs) were synthesized by combustion method, in-house as described in,[20] by heating a solution of 3569.88 mg of Zinc Nitrate Hexahydrate ($Zn(NO_3)_2 \times 6H_2O$) and 1200 mg of Sucrose ($C_{12}H_{22}O_{11}$) with 3 mL of DI water in a beaker on a hot plate. The zinc nitrate decomposition generated brownish-yellow gases and eventually a blackish-brown foam. The foam was stirred for approximately 20 minutes, allowing the carbon to combust away as carbon dioxide, forming the yellowish-white ZnO NP powder. The hot plate was turned off, and the NPs turned white as they cooled.

X-Ray Diffraction (XRD) characterization and Scanning Electron Microscopy (SEM) were conducted on the synthesized ZnO NPs to confirm composition and determine nanoparticle size following previously published guidelines.[23] Commercially available TiO_2 was used as a control for the in-house synthesized ZnO NPs in this study. Terephthalic Acid (TA) was used to confirm radical generation from the NPs.

XRD and SEM of Nanoparticles

All gel samples were air-dried and subjected to XRD in a powder form. The phase and crystal structure of the nanoparticles were analyzed using XRD, and the patterns were obtained using the Rigaku Benchtop powder X-ray diffractometer (Mini Flex II) using Cu-Kα radiation (l=1.5418 Å) at room temperature. The scan was carried out over an interval of 20°– 80° (2-θ range), step size of 0.02°, and a scan rate of 0.6°/min for all the measurements. The crystallite size was determined to be 19 nm using the Debye Scherrer Relation given as;

$$D = 0.9\lambda/\beta\cos\theta \quad (1)$$

where D is the crystallite size, λ (CuKα) – 1.5406 Å, β is the full width at half maximum and θ is the diffraction angle.

The microstructure of the ZnO and TiO_2 NPs were imaged using SEM (Hitachi 4800) in the secondary electron scattering mode, and the size was measured using ImageJ software. The samples were sputter-coated with gold, prior to imaging, to avoid charging effect.[24]

Radical Generation Probe Test

A $5x10^{-3}$ M concentration of Sodium Terephthalate (NaTA) was prepared by the stoichiometric addition of sodium chloride and terephthalic acid. One milliliter of NaTA was added to wells with 5 mg each of either ZnO or TiO_2 NPs and placed on a shaker (IBI Scientific, Dubuque, IA, USA) for 10 min to allow reaction. The plate was placed in the Intelliray 600 UV chamber (Uvitron Intelliray 600 Curing Unit, West Springfield, MA) fitted with a UV bulb (Uvitron UVA 600-Watt Halide Lamp, 365 nm) for 5 minutes at 100% intensity to release hydroxyl radicals. NaTA reacted with the hydroxyl radicals to form 2-hydroxy terephthalate, a fluorescent probe

for the detection of the hydroxyl radicals.[25] One hundred microliters of samples were placed in black, clear-bottom 96 well microplates (Corning Inc., Corning NY). The plates were read using Fluoroskan™ Microplate Fluorometer with Ascent™ Software (Thermo Scientific) with excitation and emission wavelengths of 355 nm and 444 nm, respectively.

Preparation of Alginate Gels Impregnated with ZnO NPs

The ZnO alginate gel solution was prepared in 50 mL centrifuge tubes using the materials listed in Table 1. A separate solution of 0.25 M Calcium Chloride ($CaCl_2$) crosslinker was prepared by combining 254 mg of $CaCl_2$ in 8 mL of deionized (DI) water, as done earlier.[26] One hundred microliters of crosslinker were added per mL of DI water along with the corresponding ZnO or TiO_2 NPs for each solution to partially crosslink the alginate for maintenance of structural fidelity when bioprinted. The NPs were thoroughly mixed into the $CaCl_2$ and H_2O solutions using a vortex mixer to avoid settling of NPs. This was followed by the immediate addition of alginate and vortex mixing for 10–20 seconds or until the contents of the tube appeared visually homogeneous.

Gel Fabrication

The gel mixtures were then loaded in 10 mL syringes (ThermoFisher Sci.) for 3D bioprinting. Controls were manually casted and shaped within molds by extrusion from the syringes, as well. Four varying groups were used in this study, with the gel solutions being, alginate only, alginate ± 0.5% w/v ZnO NPs, alginate ± 1% w/v ZnO NPs, and alginate ±1% w/v TiO_2. These doses were finalized based on guidance derived from other published works where a comprehensive dose range of ZnO NPs (0.05–1% w/w) was evaluated.[27] The results of this investigation showed significant hemostatic ability, biocompatibility, and antimicrobial effects on bacterial pathogens for these nanocomposites at 1% ZnO NPs compared to commercially available alginate dressing.[28,29]

3D Printed Gels

Ten-milliliter syringes loaded with the gels were fitted with 24-gauge steel tip needles (HUAHA, Amazon) and placed in a 3D extrusion bioprinter (BioBot 1, Allevi, PA, USA; Cellink, MA, U.S.A.). Lattice cube and cylinder.stl files were designed with the SolidWorks program. Structure dimensions were modified and converted to g-code with Repetier Host software, as required for each experiment. 3D constructs were printed onto petri dishes at 138–207 kPa.[30] Once printed, the gels were each cross-linked again with 100 µL of 0.25 M $CaCl_2$ for 20 minutes and washed with 1X-PBS to remove residual $CaCl_2$.

Manually Casted Gels

Silicone putty molds of 10 mm diameter and 2 mm depth were created according to product package instructions (EasyMold® Silicone Putty, Castin' Craft®). The gels were manually extruded through the 10 mL syringes into the molds. Once casted, they were cross-linked in 100 µL of 0.25 M $CaCl_2$ for 25 minutes and washed with PBS, as done earlier.[31]

Scanning Electron Microscopy (SEM) of the Composite Gels

To assess and compare the dimensions of the pores within the 3D printed and manually casted gels, cross-sectional images were obtained via SEM, as described in previously published studies.[30–33] Samples were crosslinked, placed in 193.15°K overnight, lyophilized, and sliced to reveal a cross-sectional area. These sections were sputter-coated (Gatan Model 682 Precision etching coating system, Pleasanton, CA, USA) and viewed with SEM (S-4800, Hitachi, Japan). Image J software was utilized to measure the average pore diameter.

Swelling Assay

The swelling capacity of the 3D printed, and manually casted gels were analyzed via a swelling assay.[33] 3D

Table 1 Measured Amounts of DI H_2O, 0.25 M $CaCl_2$, ZnO, TiO_2, and Alginate Constituting the Formation of Each Gel Sample, Alginate Only, Alginate + 0.5% ZnO, Alginate + 1% ZnO, and Alginate + 1% TiO_2

Solution	DI H_2O (mL)	0.25 M $CaCl_2$ (uL)	ZnO (g)	TiO_2 (g)	Alginate (g)
Alginate only	4.800	500	0	0	0.20
Alginate + 0.5% ZnO	4.775	500	0.05	0	0.20
Alginate + 1% ZnO	4.750	500	0.10	0	0.20
Alginate + 1% TiO_2	4.750	500	0	0.10	0.20

printed lattice and manually casted structures were crosslinked and placed in a desiccator for 18 hr. Once dried, the samples were weighed to find the initial dry weight (W_0), then placed in PBS to allow swelling. The samples were then weighed (W_t) every 24 hr for 5 days to track the uptake of the solvent within the samples. The following formula for degree of swelling (Ds) was used to calculate the swelling ratio:

$$D_s = \frac{W_t - W_0}{W_0} \quad (2)$$

Extent of Degradation

To assess the physical integrity and stability of the bioprinted gels, they were tracked by phase-contrast imaging over time. Cylindrical-shaped disks (6-mm diameter) were printed and crosslinked, then washed in PBS. The gel disks were then placed in a 12 well plate and covered in 500 µL of PBS, at all times. For the following 5 days, the gels were imaged every 24 hr.

Rheological Analysis

To determine the rheological parameters of the gels, shear rheometry analysis was performed on both 3D printed and casted gels. A biopsy punch was used on gels to obtain 8 mm discs of 1 mm height, which were then placed in 1X PBS to swell to equilibrium. Using Anton-Paar MCR101 rheometer (Anton-Paar, Graz, Austria) with an 8-mm parallel plate geometry, oscillatory shear stress analysis was conducted at 1% L.V.E. strain from 0.05 to 50 Hz. All moduli, along with complex viscosity, are reported at 1.99 Hz.

Antibacterial Testing

For confirmation of antibacterial properties of the NP encapsulated gels, a bacterial test was conducted on *Staphylococcus epidermidis* (*S. epidermidis*), comparing U.V. exposed and non-exposed gels. All gels were autoclaved prior to being casted. Gels were printed into 6 mm disks, crosslinked, and placed in 48-well microplates (Corning Inc., Corning NY). Two hundred microliter of nutrient bacterial broth were pipetted into each of the wells. An erythromycin disk placed within the center of the well served as a control in each group. The plate designated for U.V. exposure was placed in the Intelliray 600 for 5 minutes at 100% intensity, while the other plate was maintained in surrounding room light. The *S. epidermidis* was diluted by using an inoculation loop to transfer 10 µL of bacteria into 5 mL of nutrient broth. Each well had 400 µL of the bacterial broth added to it. The plates were then incubated at 37°C for 24 hr. At 24 hr and 48 hr after initial incubation, 100 µL of each sample were transferred to a clear 96 well plate (Corning Inc., Corning NY) and placed in the Molecular Devices VersaMax UV/Vis plate reader with VersaMax SoftMax Pro® software (Molecular Devices, L.L.C. San Jose, CA) to measure the optical density at 600 nm wavelength. This experiment was repeated twice (n=2).

Cytocompatibility

The cytocompatibility of the NP encapsulated gels were assessed by culturing mitomycin-C treated STO (MITC-STO) fibroblast cells (Millipore Sigma, Burlington, MA, USA) in complete growth medium (C.G.M.; Dulbecco's Modified Eagle's Medium/Nutrient Mixture F-12 Ham with 15 mM HEPES) for direct experimental use after a 24 hr incubation (310.15°K, 5% CO_2). To the CGM., 12.5% fetal bovine serum and 1% penicillin-streptomycin were added. Samples were printed in the form of cylindrical discs using a sterile environment. Samples were placed in a 48-well microplate and 200 µL DMEM media was added to each well. The plate was placed in a microprocessor-controlled light-curing system (IntelliRay 600) for a five-minute UV irradiation. Samples were transferred to a sterile 48-well plate in their respective wells containing cells, including a control group with cells containing no gels and restricting UV exposure to observe general fibroblast proliferation. Fibroblast cells were seeded at a density of 2×10^5 cells/mL within the 48-well plate. Each well had 200 µL of DMEM media added, and the plate was incubated 24 hr (310.15°K, 5% CO_2). Cell viability was assessed using Calcein AM (live) stain and Ethidium Homodimer-1 (dead) stain (LIVE/DEAD® Viability/Cytotoxicity Kit for mammalian cells, Molecular Probes). Imaging (ZEISS AxioPhot Fluorescent Microscope, Germany) was performed to confirm the retention of viable cells and the presence of dead cells in each sample. All images collected using the ZEN. Digital Imaging Software underwent quantitative analysis through FIJI (Image J Digital Imaging extension). Particle analysis of masked images of Calcein AM (green threshold) and Ethidium Homodimer-1 (red threshold) measured the cells observed in the respective wells of each gel group.[34] The percentage of live or dead cells was obtained based on the following equation; this was determined from the average particle count of each sample (n = 2).

$$\text{Number of Live or Dead Cells}(\%) = \left(\frac{\text{Number of particles in green or red threshold image}}{\text{Total number of particles in green and red threshold images}} \right) x100\% \quad (3)$$

Humidity Sensor

To quantify moisture retention for the hydrogels over a 6-day period, a monitoring system, composed of an ELEGOO Uno R3 Board ATMega328P ATMEGA16U2 microcontroller, D.H.T. 11 humidity and temperature sensor module, Adafruit MicroSD card breakout board, and an LCD screen all of which was acquired from Adafruit Industries (NY, U.S.A.), were programmed through the Arduino software to take measurements of the DHT11 module readings every 30 minutes and log them onto the SD card. For each sample type, a 16 mm x 12 mm 3D printed lattice hydrogel sheet was placed atop the DHT11 humidity sensor and enclosed within a 35 mm petri dish to generate an isolated environment . To further diminish outside air exposure, the petri dish was wrapped extensively with parafilm to prevent any openings between the dish enclosure and the wire protrusion of the sensor. The microcontroller was connected, and measurements began at the placement of the hydrogel atop the DHT11 sensor, displaying humidity and temperature readings through the LCD screen. The data were evaluated based on relative humidity (RH) percentage recorded on the DHT11 module, calculated from the following equation:

$$RH(\%) = \left(\frac{\text{Density of water vapor}}{\text{Density of water vapor at saturation}} \right) x100\% \quad (4)$$

Each hydrogel sample was left atop the sensor for 6 days. This experiment was conducted twice (n = 2).

Statistical Analysis

All experiments were performed with sample groups of at least three repeats (n=3) unless otherwise mentioned. Data are presented as the mean ± standard deviation (SD). Two-way ANOVA, followed by Tukey's post-test for multiple comparisons, was performed to determine the statistical significance between individual sample groups with significance set at $p< 0.05$.

Results and Discussion

Characterization of NPs

Figure 1A shows the SEM micrographs of the prepared ZnO NPs. The particles were spherical in shape and of uniform size distribution. The measured particle size was in the range of 4–6 nm. NPs are known to have effective interaction with bacteria if the particle size is less than or equal to 30 nm.[35] The smaller the particles are, the larger their surface area to volume ratio. Here the particle size of the ZnO NPs is approximately 5 nm, effectively increasing the surface area for effective interaction. Supplementary Figure S1A shows the SEM micrographs of the TiO_2 NPs. The micrograph at a lower magnification is given as the inset. The TiO_2 NPs were non-uniform in nature with varying sizes, and the particle size range was from 7 to 23 nm as calculated.

The phase and crystallinity of the prepared ZnO NPs were studied and are shown in Figure 1B. The diffraction peaks were sharp and intense, suggesting that the nanoparticles are highly crystalline and match very well with the standard data card (JCPDS – 80-0075; a = 3.259 Å and c = 5.209 Å) of hexagonal phased ZnO. There is no evidence of any impurity phase present in the sample. Similarly, the X-ray diffractograms of TiO_2 NPs are shown in Supplementary Figure S1B. The characteristic peaks match with the anatase phase of the TiO_2 (JCPDS card No. 21–1272). The crystallite size was calculated using the Debye Scherrer relation and was observed to be 20 nm.

Hydroxyl Radical Generation

By comparing the fluorescence of the nanoparticles in NaTA and DI water, the comparative release of hydroxyl radicals was ascertained. Data suggested a highly significant difference ($p<0.001$) in fluorescence when either ZnO or TiO_2 were added to the NaTA compared to when the NPs were added to DI water (Figure 2). Measuring the emission of the 5 mM NaTA without any NPs added, showed similar results to those obtained from NPs in water. This further supported the occurrence of the reaction being the transformation of NaTA to the fluorescent 2-hydroxy-terephthalate in the presence of hydroxyl radicals.[25] There was, however, the only slightly discernible difference in fluorescence between the ZnO-NaTA and TiO_2-NaTA samples (not statistically significant). This result ensured the generation of free hydroxyl radicals from the NPs, which is the primary mechanism by which the ZnO NP impregnated alginate gels exhibit antibacterial properties. Studies suggest that ZnO

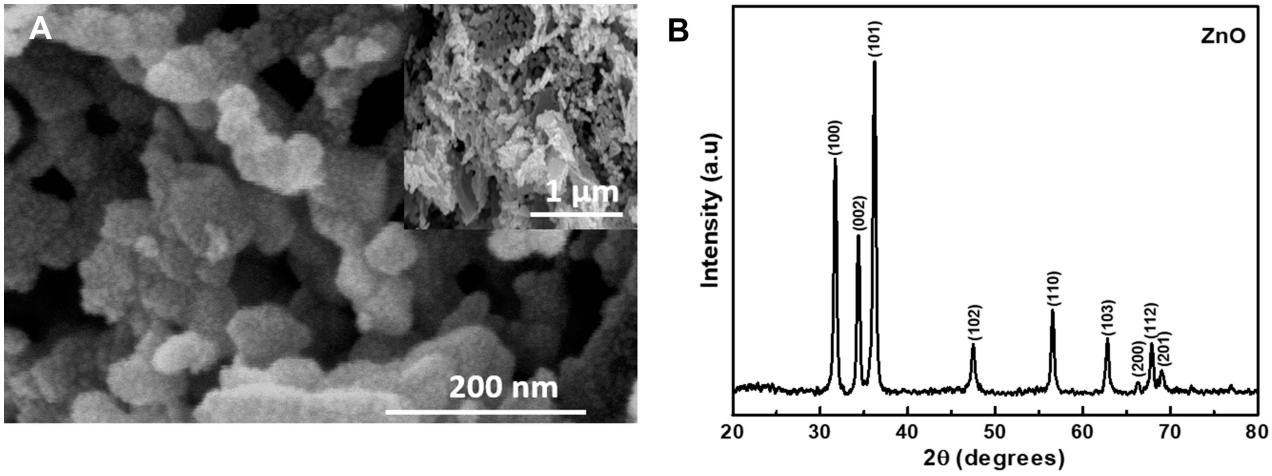

Figure 1 ZnO Characterization. (**A**) SEM micrographs of ZnO nanoparticles at different magnifications. The inset shows the low magnification image of ZnO nanoparticles. (**B**) XRD patterns of ZnO nanoparticles prepared in-house.

NPs disrupt the cell membrane to cause cell death.[35] This mechanism is enhanced by the generation of reactive oxygen species (ROS.) such as hydroxyl radicals.[35–37]

Visual Appearance, Microstructure, and Composition of Gels

By way of visual comparison, 3D printed gels with and without NPs looked distinctly different from their manually casted counterparts (as outlined in Supplementary Figure S2), due to the presence of a defined lattice structure, as seen in Figure 3A–D compared to Figure 3E–H. Supplementary Figure S3 details the preparation of the NP incorporated alginate gel prior to either casting or printing into scaffolds. It may be noted that gels containing doses of NPs lower than 0.5% w/v were applied towards printing but exhibited poor printability and shear thinning characteristics due to the extremely low density of the NP when mixed within the alginate gel solution, prior to printing and crosslinking (data not shown).

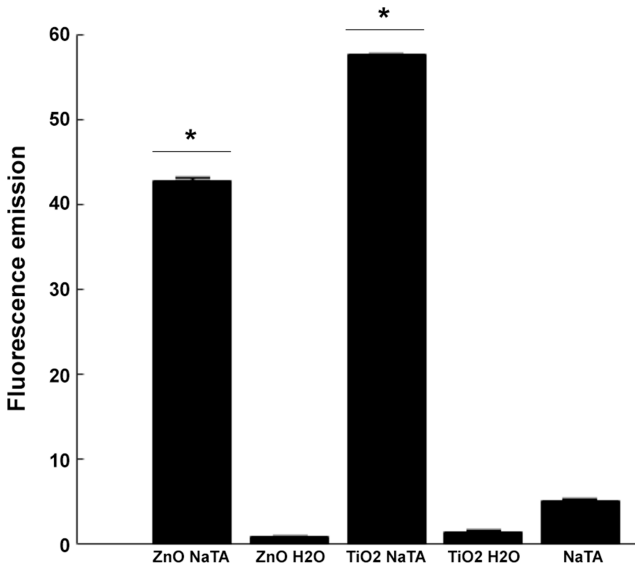

Figure 2 Radical Generation Probe Assay. Chart comparing fluorescence emission of ZnO and TiO_2 nanoparticles in Sodium Terephthalate (NaTA) and DI H_2O and negative control NaTA. *Indicates statistically significant difference ($p<0.05$).

SEM was performed on all the samples manufactured by two different methods (ie, 3D printed vs manually cast) to compare morphological features of constructs made using both techniques. Upon visual inspection of the different sample images acquired using SEM, it was distinguishable that the 3D printed samples exhibited smaller sized and homogeneously distributed pores (Figure 4A–D) compared to the manually casted samples (Figure 4E–H). It was also observed that the different gel-formation methods played a significant role in the relative porosity and morphological roughness present on each sample, pointing towards a higher degree of porosity and uneven morphology when samples were casted (Figure 4). This may be attributed to the Surface Area to Volume ratio (SA:V), which plays a significant role in the rate of crosslinking and, as a consequence, the crosslinking density of the sample. At higher SA:V ratios, crosslinking was observed to take longer to achieve complete gelation. Additionally, a higher degree of crosslinking has been observed to reduce pore size in alginate samples,[34] as well as enhancing its stability[26] by reducing the degree of swelling when exposed to physiologically similar conditions. We attributed the stability to a reduced ion diffusion through the smaller pores present in 3D printed samples due to a high SA and smaller V. The reverse was true for the casted samples, for the most part, demonstrating a higher V and a

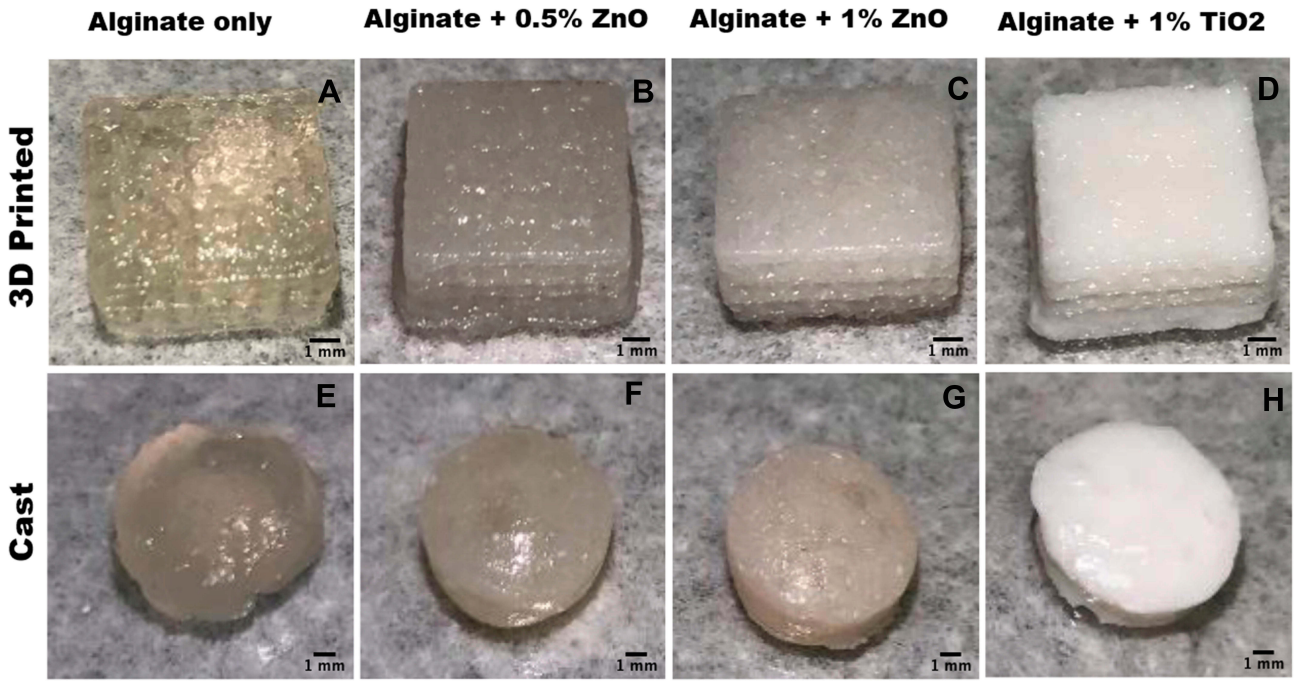

Figure 3 (**A**–**D**) depict 3D printed lattice structures. (**E**–**H**) portray manually casted structures. Scale bar in all images depict 1 mm.

relatively similar SA. These results confirmed the rationale for adopting an advanced manufacturing technique such as 3D bioprinting for making these NP-based hydrogel constructs.

Among the 3D printed sample group, statistical analysis showed a significant increase in average pore diameter ($p<0.002$) due to the addition of NPs to the alginate (Figure 4I). Among the manually casted gel group, there was no statistical difference between the pore dimensions across all samples.

Supplementary Figure S4 shows the XRD patterns of pristine sodium alginate gel and sodium alginate gel infused with ZnO NPs.[38] It can be observed that the ZnO infused sodium alginate gel gives the characteristic peaks of ZnO NPs, also retaining the characteristics of sodium alginate. As the concentration of ZnO NPs is increased in the infusion, the characteristic peaks of ZnO become more prominent, confirming the presence of ZnO NPs.

Swelling and Degradation Behavior of Gels

The swelling behavior of the manually casted and 3D bioprinted gels over a period of 5 days was compared, as shown in Figure 5. In the manually casted sample groups (Figure 5B), a significant difference in swelling ratios were observed ($p<0.001$), while only TiO_2 showed significantly smaller ratio in comparison to the alginate only and 0.5% ZnO samples ($p<0.05$) in the bioprinted gel samples (Figure 5A). This shows a more consistent pattern of swelling over a longer period of time among the 3D printed samples, indicating the potential for a more reliable scaffold for wound healing. Overall, the manually casted samples showed a lesser degree of swelling than those bioprinted, suggestive of a more readily available swelling capability when samples are bioprinted, most likely attributed to its lattice structure.[32] Once in contact with an exuding wound, a particle trade response happens between the calcium particles in the dressing and sodium particles in serum or wound liquid. When a significant proportion of the calcium ions on the template have been replaced by sodium, the structure swells and partially dissolves, forming a gel-like mass. This structure allowed for better diffusion and uptake of the solvent. In the process of wound healing, applying these characteristics will play an essential role in allowing the diffusion of nutrients and controlling any flow of wound exudates or secretions. Furthermore, when taking into consideration the swelling results and pore size studies, we were able to confirm the effect of the difference in manufacturing methods used to make the gels in this study.

As seen in Supplementary Figure S5, upon visually tracking the bioprinted samples in PBS over a period of

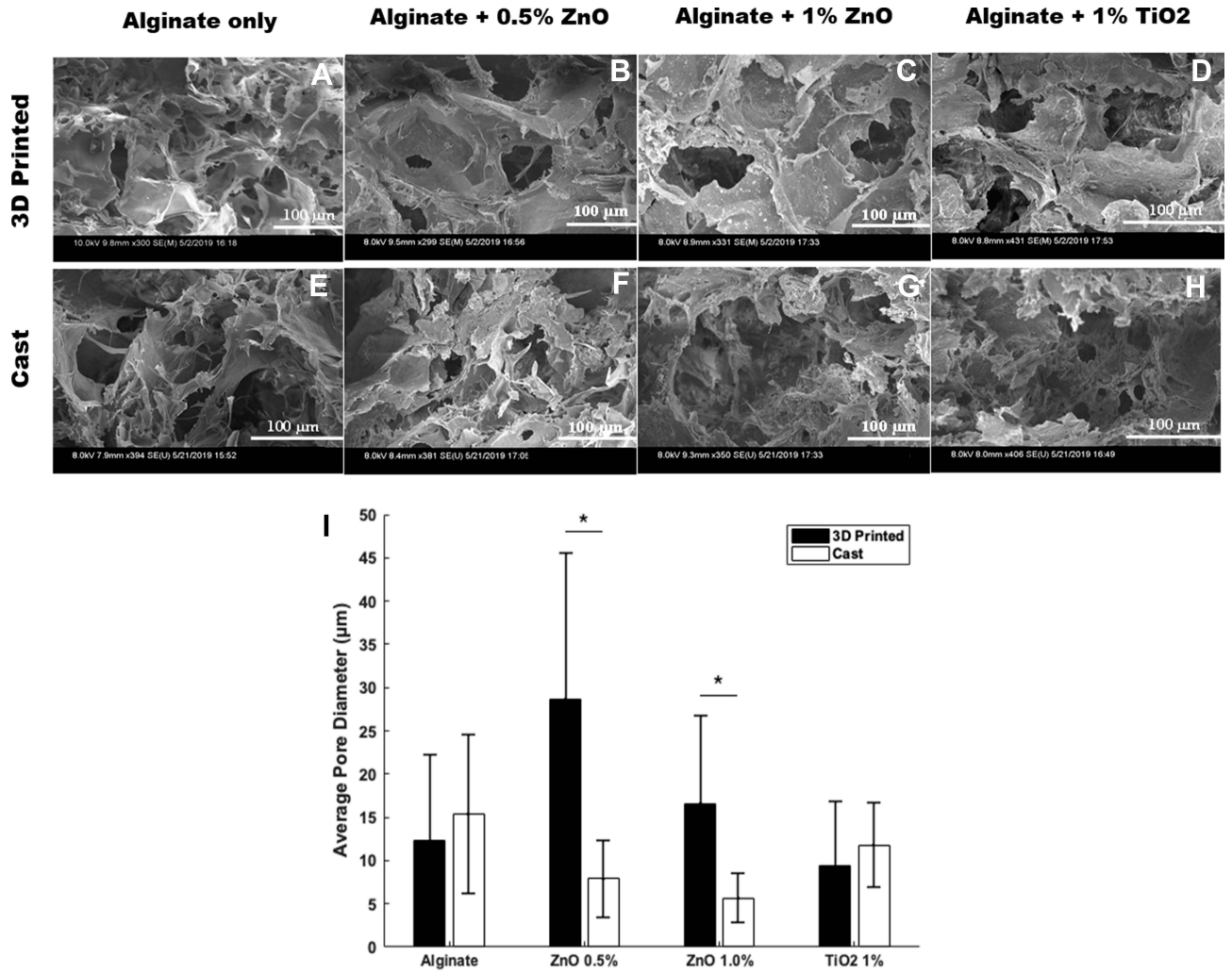

Figure 4 Scanning Electron Microscopy (SEM) Imaging and Analysis. Cross-sectional SEM imaging of (**A**–**D**) 3D printed gels and (**E**–**H**) manually casted gels. (**I**) Graph depicting the average pore diameters of both 3D printed and manually casted gels. Scale bar in all images depict 100 µm. *Indicates statistically significant difference ($p<0.05$).

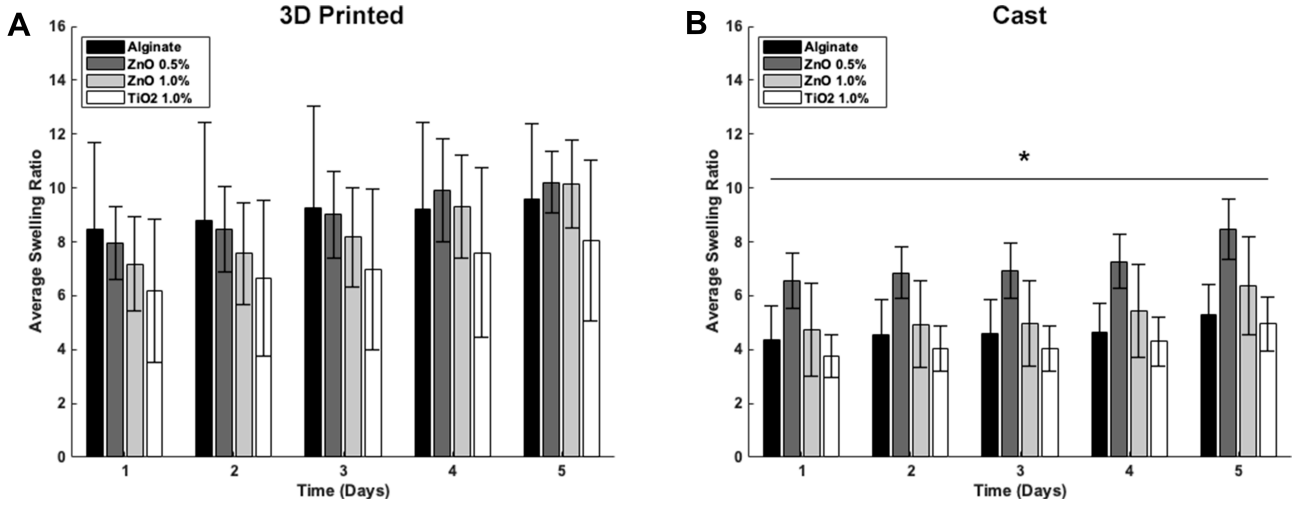

Figure 5 Swelling and Degradation Assay. (**A**) Swelling analysis of 3D printed gels over 5 days. (**B**) Swelling analysis of manually casted gel over 5 days. *Indicates statistically significant difference ($p<0.05$).

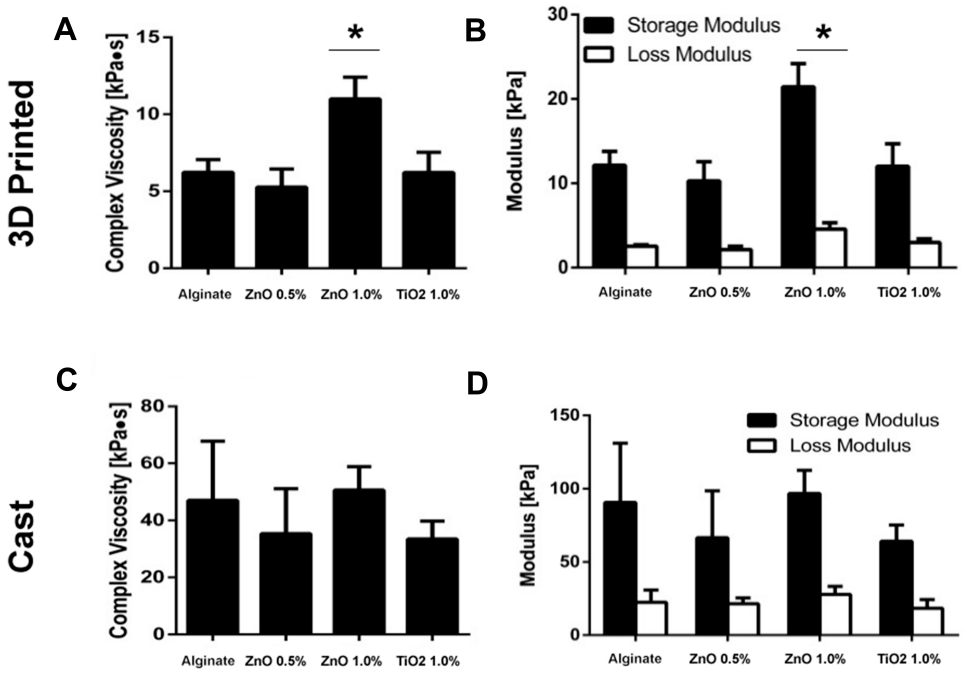

Figure 6 Rheological Analysis. Quantification of complex viscosity and moduli measured at 1.99 Hz of 3D printed gels (**A** and **B**) compared to casted gels (**C** and **D**). *Indicates statistically significant difference ($p<0.05$).

28 days, a difference in degradation was seen in the ZnO samples in comparison to the alginate only and TiO_2 samples. Within 7 days, the alginate gel samples began losing structural fidelity, and TiO_2 had degraded extensively. Conversely, both the 0.5% ZnO and the 1% ZnO samples maintained their structures for a more extended period of time, remaining intact throughout the 28 days. Such longevity of the 3D printed gels is due to the combined crosslinking of both calcium and zinc ions to alginate.[39] Along with zinc's binding site to alginate being different from that of calcium's, zinc ions are also less selective, presumably leading to the increased crosslinking of the alginate gels in our study by the ZnO NPs.[39]

Mechanical Properties of the Gels

Samples of gels that were bioprinted into a 3D lattice or manually casted disks showed predominantly elastic behavior, as seen in Figure 6. Storage and loss modulus for each sample with varying ZnO concentrations were determined using shear rheology, utilizing a frequency sweep between 0.5Hz and 50Hz. Manually casted gels displayed no significant difference among samples in complex viscosity, storage, and loss modulus (Figure 6C and D). However, all of the manually casted samples had higher stiffness values, indicated by higher Elastic Moduli measurements, than their 3D printed counterparts, as shown in Table 2, possibly due to the uncontrolled forming of gels onto a casted mold, resulting in disks having increased mechanical properties. In addition, the manually casted gels were solid throughout, resulting in their increased rigidity when compared to the bioprinted gels with a lattice structure. Statistical analysis showed a significant increase in complex viscosity ($p<0.002$) as well as the storage and loss modulus ($p<0.003$) in bioprinted gels

Table 2 Elastic Modulus and Complex Viscosity Values Obtained from the Rheological Analysis of Both Manually Cast and 3D Printed Alginate Only, Alginate + 0.05% ZnO, Alginate + 1% ZnO and Alginate + 1% TiO_2 Scaffolds

Sample	Elastic Modulus (KPa)	Complex Viscosity (KPa.s)
Manually cast		
1. Alginate only	280.5 ± 123.47	47.03 ± 20.78
2. Alginate + 0.5% ZnO	210.82 ± 93.92	35.37 ± 15.76
3. Alginate + 1% ZnO	302.41 ± 49.06	50.63 ± 8.23
4. Alginate + 1% TiO_2	200.28 ± 37.13	33.53 ± 6.21
3D printed		
1. Alginate only	37.18 ± 4.95	6.23 ± 0.83
2. Alginate + 0.5% ZnO	31.48 ± 6.98	5.27 ± 1.17
3. Alginate + 1% ZnO	65.73 ± 8.53	10.99 ± 1.41
4. Alginate + 1% TiO_2	37.17 ±7.81	6.22 ± 1.31

with the addition of 1% ZnO (Figure 6A and B). This is indicative of the additional crosslinking provided by zinc ions on alginate.[39] However, this may be beneficial towards the retention of structural stability and possession of enhanced mechanical properties by the nanocomposites, as also shown by others.[40] The addition of TiO_2 appeared to have no effect on the mechanical properties of the gels.

Bacterial Growth Inhibition

In an ideal scenario, the ZnO NP infused gels should inhibit the growth of bacterial production largely compared to the TiO_2 NP-gels. To explore this, both U.V. exposed and unexposed ZnO laden gels were tested for antibacterial properties in *S. epidermidis* bacterial broth, as illustrated in Figure 7A. Both 0.5% ZnO and 1% ZnO groups of gels showed a comparable antibacterial activity to the erythromycin control, a well-established antibacterial treatment (Figure 7B). The TiO_2 samples showed similar behavior to the control alginate, which differed from the ZnO and erythromycin samples' bacterial growth-inhibiting performance. This can be attributed to ZnO NPs' consistently smaller average size when compared to TiO_2 NPs, with size possibly affecting the ability to invade bacterial cells.[30] In general, the U.V. irradiation demonstrated an effect on the optical density ($p<0.05$), signaling the decreased presence of bacteria. This reinforces the concept of photocatalytically activated formation of hydroxyl radicals leading to bacterial cell death.[36] *S. epidermidis* is a common bacterium on the skin, making it a likely cause of infection and primary target for this study. In the occurrence of a wound, the bacteria can travel from the skin into the body, much as it would in other cases of trauma or surgery.[41] The antibacterial properties of ZnO were evident in the ability of the ZnO gels to produce a low optical density of the bacterial inoculated broth compared to alginate samples. This reveals our ZnO gels to have great potential to be used as an antibacterial dressing for chronic wound healing.

Cytocompatibility with Fibroblasts

Although bacterial growth-limiting, in order to promote their use as wound healing templates, the NP infused, gels should be completely safe when added to growing cell cultures. In order to explore their cytocompatibility with fibroblasts, MITC-treated fibroblasts were used in this study. Post-treatment with MITC, the cells were growth-arrested and served as an ideal basis for studying the resultant cytotoxicity when in contact with the NP infused gels. By way of visual comparison after live/dead staining, cells retained viability in all samples; however, a higher number of dead cells were existent in samples cultured in the presence of NP encapsulated alginate gels (Figure 8A–J). Quantified results are depicted in Figure 8K. Due to the homogenous distribution in the data set, transformation to normality could not be achieved, requiring independent assessment of each experimental group. This was achieved through Post-Hoc confirmation of the Kruskal Multiple Components test. The percent cell viability showed no significant difference ($p > 0.05$) between any gel samples and the control group with no gel (Figure 8K). No significant difference across the five groups in this study revealed uniform cell viability at 24 hr of culture, signifying an improbability of cytotoxicity across experimental groups.

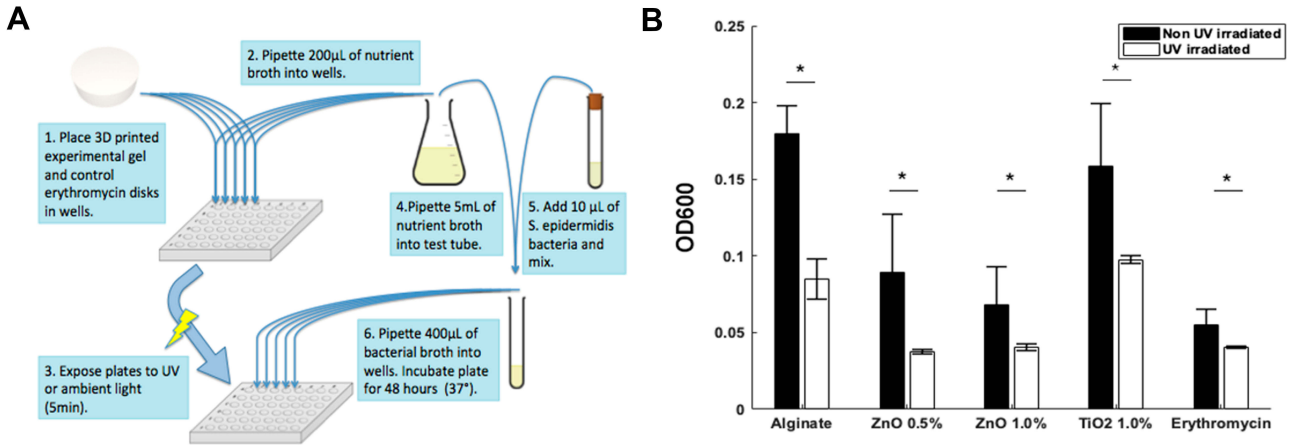

Figure 7 Bacterial Testing. (**A**) Schematic of bacterial testing steps conducted on gels in *S. epidermidis* bacterial broth. (**B**) Optical density at 600 nm after 48 hr of gel samples in *S. epidermidis*. *Indicates statistically significant difference ($p<0.05$).

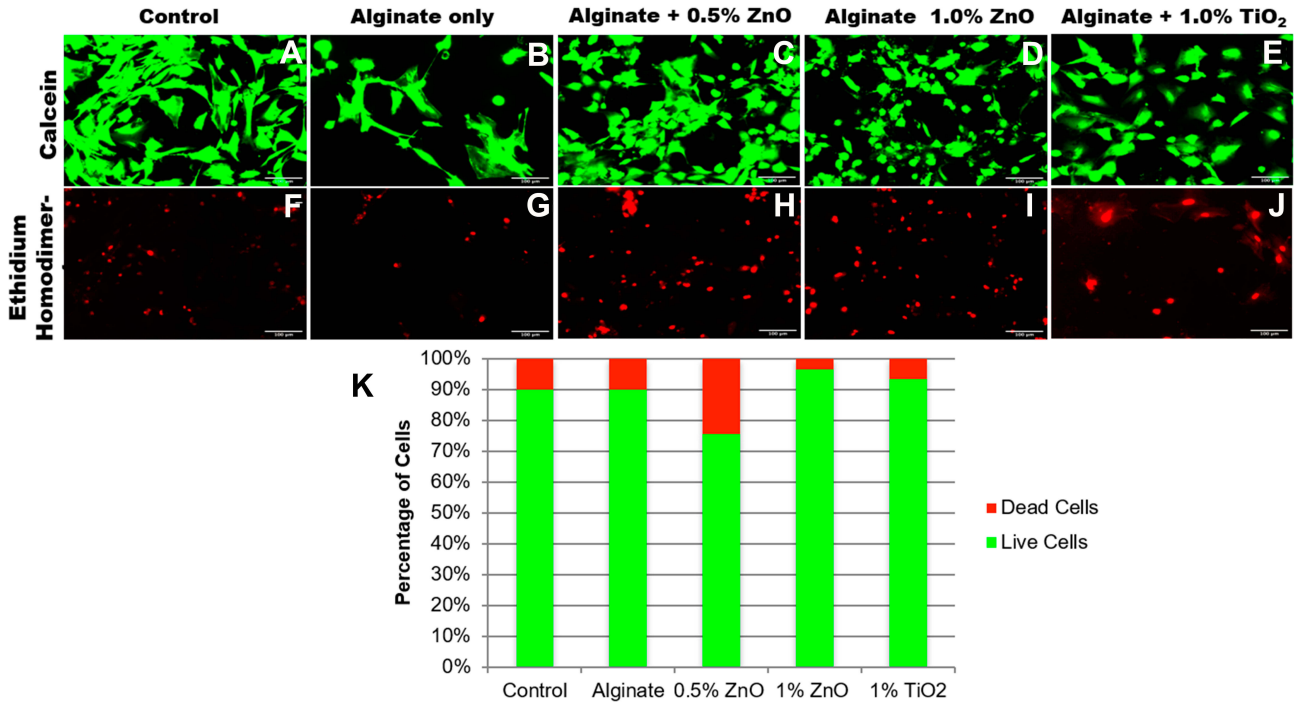

Figure 8 Cytocompatibility. Confocal Imaging of LIVE/DEAD Cell Viability Assay for CF-1 MEF IRR 2M mammalian fibroblast cells, when cultured along with the 3D printed discs in the same wells. The images consisted of Calcein (**A**–**E**), and EtHD-1 (**F**–**J**) treated cells. Viability was quantified after a 24-hr period as a LIVE/DEAD cell percentage (**K**) based on particle analysis obtained through FIJI color threshold segmentation. Scale bar in all images (**A**–**J**) depict 100 μm.

As seen in Figure 8K, 1% ZnO (88.4%) and 1% TiO_2 (93.4%) had similar percentages (± 5%) of live cells at identical concentrations, congruent with the premise of nanoparticle dispersion influencing cell viability.[42,43] It is unknown whether a correlation to toxicity exists due to the concentration of NPs. However, cell viability was assessed of the photocatalyzed ZnO NPs, implying the ZnO NPs toxicity remains under the threshold of substantial cell damage. Future studies considering nanoparticle concentration would reveal the optimal amount; ideally, at a lower concentration of ZnO NPs more cell viability would induce cellular proliferation, an existent attributed correlation.[27,36]

Retention of Humidity

By using a humidity monitoring and logging microcontroller system (Figure 9A) over six days, a 1% ZnO and alginate hydrogel were revealed to have statistically significant higher moisture retention in comparison to the alginate only gel, suggesting a correlation between the structural property and incorporation of a larger quantity of ZnO NPs. A timeline of 8-hour time points shows prolonged R.H. percentages (Figure 9B) for 0.5% ZnO and 1% ZnO with an observed difference of 11.73%. Similarly, 0.5% ZnO and 1% TiO_2 demonstrated comparable trend lines, supported by within range critical values with an observable difference of 2.49%. Quantitative analysis upon normal distribution of data, by the Kruskal–Wallis and Post-Hoc Kruskal Multiple Components tests, showed an observed difference of 37.31% between 1% ZnO and alginate, a difference of 25.59% between 0.5% ZnO and alginate, and a difference of 23.10% between 1% TiO_2 and alginate. Divalent ions crosslink alginate, producing an "eggbox" structure. With Zn ions being less selective that Ca ions, there is a greater extent of interaction and increased crosslinking of the alginate. This leads to less permeability in an increased concentration of Zn cations and, therefore, less loss of water.[39]

Study states that ZnO crosslinked alginate had more stable bonds and decreased pore size with less nitrogen loss.[44] This can be translated to the results of our ZnO scaffolds retaining moisture longer, due to those smaller pores and stability of the structure. Optimizing ZnO concentration with this ability is pertinent towards producing a moist microenvironment favorable to healing wounds by creating a bioactive cell membrane that diminishes the expression of scar tissue formation[45] and works in conjunction with the advantageous properties of alginate wound dressings.[13,14]

In summary, the hydroxyl radical assay data demonstrated the sufficient production of hydroxyl radicals from

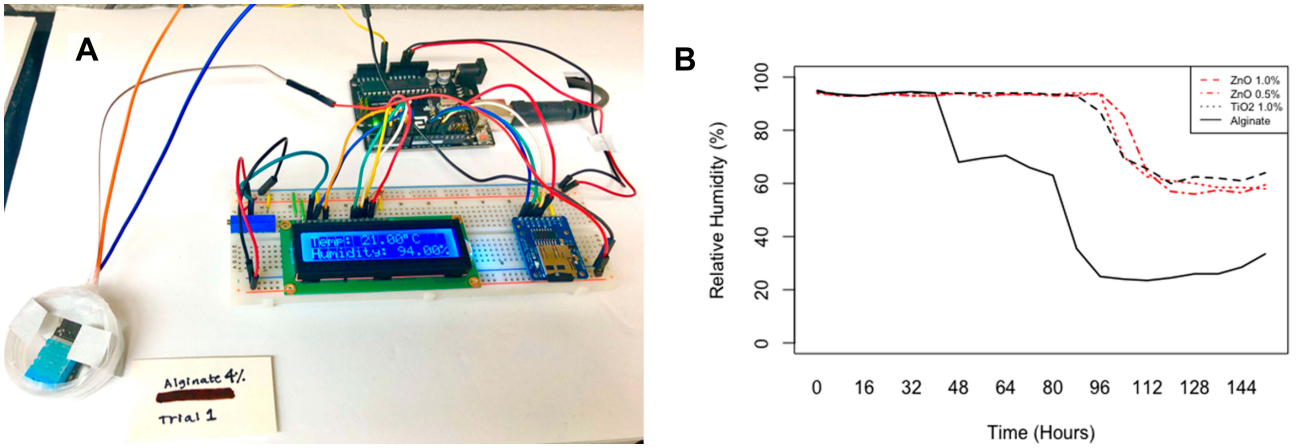

Figure 9 Moisture retention evaluation of hydrogels based upon setup (**A**) of ELEGOO Uno R3 Board ATMega328P ATMEGA16U2 monitoring by a (16x2) L.E.D. screen of DHT11 temperature and humidity module encapsulated within a petri dish and parafilm isolated, programmed for data collection from Adafruit MicroSD card breakout board at 30 minute time points for the course of 7 days. Timeline (**B**) of relative humidity (%) demonstrated at 16 hr intervals over 7 days correspondent to each hydrogel type [1% (w/v) ZnO NP –Alginate, 0.5% (w/v) ZnO NP – Alginate, 1% (w/v) TiO_2 – Alginate, Alginate only].

the combustion synthesized ZnO NPs. XRD analysis allowed for confirmation of the composition of both the NPs and the NP laden alginate gels. SEM imaging on ZnO NPs indicated an acceptable threshold for the antibacterial mechanism of the nanoparticles, which was further proven via bacterial testing on *S. epidermidis*. The size range of the ZnO NPs in this study was significantly smaller compared to other published reports, thereby implying that this nanocomposite gel would be effective compared to other's works involving ZnO NPs.[46] Rheology and SEM demonstrated the enhanced mechanical and structural properties of 3D printed, ZnO NP enriched, alginate gel scaffolds. Swelling and degradation assays and the moisture retention study on the scaffolds further verified these properties of integrity. In comparison with other published works,[47] our gels permitted retention of enhanced amounts of humidity and moisture, which implies that they may serve as efficient wound healing templates.

By way of comparison between the 0.5% and the 1% ZnO NP-based alginate gels, the samples containing 0.5% exhibited greater bactericidal and cytotoxic properties compared to the other set. This may be attributed to the release kinetics of the ZnO NPs from the alginate scaffold when placed in an aqueous environment. Since ZnO and alginate may crosslink chemically,[48] incorporation of NP amounts, greater than the optimized quantity (>0.5%) when encapsulated within the alginate, may not necessarily be as effective as the lower doses. Therefore, 0.5% ZnO NP based-alginate gels may be adopted for wound healing applications. This outcome is significant in terms of lowering the dose of ZnO NP (from 1% to 0.5%) necessary for retention of biocompatibility and antimicrobial properties in the alginate-based nanocomposites, in comparison with others works.[27] Future work will explore the choice of other hydrogel materials such as gelatin or collagen for being used as a scaffold for ZnO NP encapsulation, and their effectiveness in further lowering the encapsulation dose of ZnO NP while maintaining the same levels of antibacterial properties and biocompatibility of the resultant nanocomposites, as demonstrated in this study.

In utilizing hydrogels as a treatment for both chronic and general wound healing, the adjoining components must serve to completely replenish the dermal tissue.[49] Clinical studies on the challenges facing wound treatment extensively note constant inflammation to be a significant culprit in preventing reparation.[50] Topical zinc oxide application has been shown to increase wound healing, improved re-epithelialization, decreased rates of infection, and deterioration of ulcers.[51] By optimizing the concentration of ZnO NPs in an alginate-based hydrogel as done in this study, their incorporation fell within the cytotoxicity range that has been the primary concern for any substance formulation with topical application of ZnO alone.[48,51]

Conclusion

This study uniquely explores the 3D printing of a lattice structure, employing ZnO NP based-alginate gels, for more enhanced mechanical stability and customizability of wound healing treatments. The lattice structure is a bioinspired design based on the arrangement of the birefringent collagen fibers woven in a basket weave pattern.

Furthermore, in 3D printing, one gains the ability to manipulate the gel, making it patient-specific, while retaining reproducibility and efficiency. 3D printing of ZnO NP based-alginate gels may prove to be mechanically sturdier. Additionally, the degradation and humidity retention studies allow for the determination of the scaffold's viability over time to better define its use for patient application. The confirmation of the photocatalytic release of hydroxyl radicals adds to the antibacterial properties thought to be conferred solely by zinc ions. Furthermore, the use of the combustion method adds to the relative ease and low cost of producing ZnO. This study ultimately concludes that ZnO NP and alginate-based 3D printed lattice structures provide a viable alternative to existing chronic wound healing treatment options.

Acknowledgments

The authors acknowledge Shane C. Allen, Igor Estevao, Mauro Ruiz, Shweta Anil Kumar, and Brian Roman for their technical assistance. We also thank Moinak Joddar, a high school senior, for designing the Arduino circuit that was implemented in this study.

Funding

This work was supported by the NSF-PREM (DMR-1827745), NIH1SC2HL134642-01, and the NSF-MRI (DMR 1826268). G.F. acknowledges the National Institute of General Medical Sciences of the National Institutes of Health under RL5GM118969, TL4GM118971, and UL1GM118970.

Disclosure

The authors report no possible conflicts of interest in this work.

References

1. Hsu A, Mustoe TA. The principles of wound healing. In: *Plastic Surgery Secrets Plus*. Mosby; 2010:3–7.
2. Harrington C, Zagari MJ, Corea J, Klitenic J. A cost analysis of diabetic lower-extremity ulcers. *Diabetes Care*. 2000;23(9):1333–1338. doi:10.2337/diacare.23.9.1333
3. Dickinson LE, Gerecht S. Engineered biopolymeric scaffolds for chronic wound healing. *Front Physiol*. 2016;7:341. doi:10.3389/fphys.2016.00341
4. Albanna M, Binder KW, Murphy SV, et al. In situ bioprinting of autologous skin cells accelerates wound healing of extensive excisional full-thickness wounds. *Sci Rep*. 2019;9(1):1–15. doi:10.1038/s41598-018-38366-w
5. Mustoe TA, O'Shaughnessy K, Kloeters O. Chronic wound pathogenesis and current treatment strategies: a unifying hypothesis. *Plast Reconstr Surg*. 2006;117(7S):35S–41S. doi:10.1097/01.prs.0000225431.63010.1b
6. Loo Y, Wong YC, Cai EZ, et al. Ultrashort peptide nanofibrous hydrogels for the acceleration of healing of burn wounds. *Biomaterials*. 2014;35(17):4805–4814. doi:10.1016/j.biomaterials.2014.02.047
7. Lee KH, Ni WH, Loo MY, Hauser CA. C-Terminal residue of ultrashort peptides impacts on molecular self-assembly, hydrogelation, and interaction with small-molecule drugs. *Sci Rep*. 2018;8(1):1–14. doi:10.1038/s41598-017-17765-5
8. Wróblewska-Krepsztul J, Rydzkowski T, Michalska-Pożoga I, Thakur VK. Biopolymers for biomedical and pharmaceutical applications: recent advances and overview of alginate electrospinning. *Nanomaterials*. 2019;9(3):404. doi:10.3390/nano9030404
9. Thakur S, Sharma B, Verma A, Chaudhary J, Tamulevicius S, Thakur VK. Recent progress in sodium alginate based sustainable hydrogels for environmental applications. *J Clean Prod*. 2018;198:143–159. doi:10.1016/j.jclepro.2018.06.259
10. Alavi M, Rai M. Recent progress in nanoformulations of silver nanoparticles with cellulose, chitosan, and alginic acid biopolymers for antibacterial applications. *Appl Microbiol Biotechnol*. 2019;103(21–22):8669–8676. doi:10.1007/s00253-019-10126-4
11. Agarwal A, McAnulty JF, Schurr MJ, Murphy CJ, Abbott NL. Polymeric materials for chronic wound and burn dressings. In: *Advanced Wound Repair Therapies*. Woodhead Publishing; 2011:186–208.
12. Kazi GA, Yamamoto O. Effectiveness of the sodium alginate as surgical sealant materials. *Wound Med*. 2019;24(1):18–23. doi:10.1016/j.wndm.2019.02.001
13. O'Donoghue JM, O'sullivan ST, Beausang ES, Panchal JI, O'Shaughnessy M, O'connor TP. Calcium alginate dressings promote healing of split skin graft donor sites. *Acta Chir Plast*. 1997;39(2):53–55.
14. Paul W, Sharma CP. Chitosan and alginate wound dressings: a short review. *Trends Biomater Artif Organs*. 2004;18(1):18–23.
15. Clark RA, ed. *The Molecular and Cellular Biology of Wound Repair*. Springer Science & Business Media; 2013.
16. Guo SA, DiPietro LA. Factors affecting wound healing. *J Dent Res*. 2010;89(3):219–229. doi:10.1177/0022034509359125
17. Saghiri MA, Asatourian A, Orangi J, Sorenson CM, Sheibani N. Functional role of inorganic trace elements in angiogenesis—Part II: cr, Si, Zn, Cu, and S. *Crit Rev Oncol Hematol*. 2015;96(1):143–155. doi:10.1016/j.critrevonc.2015.05.011
18. Pasquet J, Chevalier Y, Pelletier J, Couval E, Bouvier D, Bolzinger MA. The contribution of zinc ions to the antimicrobial activity of zinc oxide. *Colloids Surf A Physicochem Eng Asp*. 2014;457:263–274. doi:10.1016/j.colsurfa.2014.05.057
19. Alavi M, Nokhodchi A. An overview on antimicrobial and wound healing properties of ZnO nanobiofilms, hydrogels, and bionanocomposites based on cellulose, chitosan, and alginate polymers. *Carbohydr Polym*. 2020;227:115349. doi:10.1016/j.carbpol.2019.115349
20. Islam MT, Dominguez A, Alvarado-Tenorio B, Bernal RA, Montes MO, Noveron JC. Sucrose-mediated fast synthesis of zinc oxide nanoparticles for the photocatalytic degradation of organic pollutants in water. *ACS Omega*. 2019;4(4):6560–6572. doi:10.1021/acsomega.9b00023
21. He P, Zhao J, Zhang J, et al. Bioprinting of skin constructs for wound healing. *Burns Trauma*. 2018;6:1. doi:10.1186/s41038-017-0104-x
22. Joshi S, Rawat K, Karunakaran C, et al. 4D printing of materials for the future: opportunities and challenges. *Appl Mater Today*. 2020;18:100490. doi:10.1016/j.apmt.2019.100490
23. Highley CB, Rodell CB, Burdick JA. Direct 3D printing of shear-thinning hydrogels into self-healing hydrogels. *Adv Mater*. 2015;27(34):5075–5079. doi:10.1002/adma.201501234
24. Zade V, Mallesham B, Shantha-Kumar S, Bronson A, Ramana CV. Interplay between solubility limit, structure, and optical properties of tungsten-doped Ga2O3 compounds synthesized by a two-step calcination process. *Inorg Chem*. 2019;58(6):3707–3716. doi:10.1021/acs.inorgchem.8b03328

25. Saran M, Summer KH. Assaying for hydroxyl radicals: hydroxylated terephthalate is a superior fluorescence marker than hydroxylated benzoate. *Free Radic Res*. 1999;31(5):429–436. doi:10.1080/10715769900300991
26. Alvarez-Primo F, Anil Kumar S, Manciu FS, Joddar B. Fabrication of surfactant-dispersed hipco single-walled carbon nanotube-based alginate hydrogel composites as cellular products. *Int J Mol Sci*. 2019;20(19):4802. doi:10.3390/ijms20194802
27. Mohandas A, Sudheesh Kumar PT, Raja B, Lakshmanan VK, Jayakumar R. Exploration of alginate hydrogel/nano zinc oxide composite bandages for infected wounds. *Int J Nanomedicine*. 2015;10(Suppl 1):53.
28. Suzuki Y, Tanihara M, Nishimura Y, et al. In vivo evaluation of a novel alginate dressing. *J Biomed Mater Res*. 1999;48(4):522–527. doi:10.1002/(SICI)1097-4636(1999)48:4<522::AID-JBM18>3.0.CO;2-O
29. Attwood AI. Calcium alginate dressing accelerates split skin graft donor site healing. *Br J Plast Surg*. 1989;42(4):373–379. doi:10.1016/0007-1226(89)90001-5
30. Anil Kumar S, Tasnim N, Dominguez E, et al. A comparative study of a 3D bioprinted gelatin-based lattice and rectangular-sheet structures. *Gels*. 2018;4(3):73. doi:10.3390/gels4030073
31. Joddar B, Garcia E, Casas A, Stewart CM. Development of functionalized multi-walled carbon-nanotube-based alginate hydrogels for enabling biomimetic technologies. *Sci Rep*. 2016;6(1):1–12. doi:10.1038/srep32456
32. Anil Kumar S, Alonzo M, Allen SC, et al. A visible light-cross-linkable, fibrin–gelatin-based bioprinted construct with human cardiomyocytes and fibroblasts. *A C S Biomater Sc Eng*. 2019;5(9):4551–4563. doi:10.1021/acsbiomaterials.9b00505
33. AnilKumar S, Allen SC, Tasnim N, et al. The applicability of furfuryl-gelatin as a novel bioink for tissue engineering applications. *J Biomed Mater Res B Appl Biomater*. 2019;107(2):314–323. doi:10.1002/jbm.b.34123
34. Jang J, Seol YJ, Kim HJ, Kundu J, Kim SW, Cho DW. Effects of alginate hydrogel cross-linking density on mechanical and biological behaviors for tissue engineering. *J Mech Behav Biomed Mater*. 2014;37:69–77. doi:10.1016/j.jmbbm.2014.05.004
35. Xie Y, He Y, Irwin PL, Jin T, Shi X. Antibacterial activity and mechanism of action of zinc oxide nanoparticles against Campylobacter jejuni. *Appl Environ Microbiol*. 2011;77(7):2325–2331. doi:10.1128/AEM.02149-10
36. Sirelkhatim A, Mahmud S, Seeni A, et al. Review on zinc oxide nanoparticles: antibacterial activity and toxicity mechanism. *Nanomicro Lett*. 2015;7(3):219–242. doi:10.1007/s40820-015-0040-x
37. Siddiqi KS, Ur Rahman A, Husen A. Properties of zinc oxide nanoparticles and their activity against microbes. *Nanoscale Res Lett*. 2018;13(1):1–13. doi:10.1186/s11671-018-2532-3
38. Finotelli PV, Sampaio DA, Morales MA, Rossi AM, Rocha-Leão MH. Ca alginate as scaffold for iron oxide nanoparticles synthesis. *Braz J Chem Eng*. 2008;25(4):759–764. doi:10.1590/S0104-66322008000400013
39. Chan LW, Jin Y, Heng PWS. Cross-linking mechanisms of calcium and zinc in production of alginate microspheres. *Int J Pharm*. 2002;242(1–2):255–258. doi:10.1016/S0378-5173(02)00169-2
40. Varaprasad K, Raghavendra GM, Jayaramudu T, Seo J. Nano zinc oxide–sodium alginate antibacterial cellulose fibres. *Carbohydr Polym*. 2016;135:349–355. doi:10.1016/j.carbpol.2015.08.078
41. Von Eiff C, Heilmann C, Peters G. Staphylococcus epidermidis: why is it so successful? *Clin Microbiol Infect*. 1998;4(6):297–300. doi:10.1111/j.1469-0691.1998.tb00062.x
42. Mendes LP, Delgado JMF, Costa ADA, et al. Biodegradable nanoparticles designed for drug delivery: the number of nanoparticles impacts on cytotoxicity. *Toxicol in Vitro*. 2015;29(6):1268–1274. doi:10.1016/j.tiv.2014.12.021
43. Moore TL, Urban DA, Rodriguez-Lorenzo L, et al. Nanoparticle administration method in cell culture alters particle-cell interaction. *Sci Rep*. 2019;9(1):1–9. doi:10.1038/s41598-018-36954-4
44. Santos Peretiatko CD, Andreza Hupalo E, da Rocha Campos JR, Budziak Parabocz CR. Efficiency of zinc and calcium ion crosslinking in alginate-coated nitrogen fertilizer. *Orbital*: *Electron J Chemi*. 2018;10:3.
45. Junker JP, Kamel RA, Caterson EJ, Eriksson E. Clinical impact upon wound healing and inflammation in moist, wet, and dry environments. *Adv Wound Care*. 2013;2(7):348–356. doi:10.1089/wound.2012.0412
46. Salama A, Diab MA, Abou-Zeid RE, Aljohani HA, Shoueir KR. Crosslinked alginate/silica/zinc oxide nanocomposite: a sustainable material with antibacterial properties. *Compos Commun*. 2018;7:7–11. doi:10.1016/j.coco.2017.11.006
47. Bajpai SK, Chand N, Chaurasia V. Nano zinc oxide-loaded calcium alginate films with potential antibacterial properties. *Food Bioproc Tech*. 2012;5(5):1871–1881. doi:10.1007/s11947-011-0587-6
48. Chopra M, Bernela M, Kaur P, Manuja A, Kumar B, Thakur R. Alginate/gum acacia bipolymeric nanohydrogels—promising carrier for zinc oxide nanoparticles. *Int J Biol Macromol*. 2015;72:827–833. doi:10.1016/j.ijbiomac.2014.09.037
49. Dimatteo R, Darling NJ, Segura T. In situ forming injectable hydrogels for drug delivery and wound repair. *Adv Drug Deliv Rev*. 2018;127:167–184. doi:10.1016/j.addr.2018.03.007
50. Larouche J, Sheoran S, Maruyama K, Martino MM. Immune regulation of skin wound healing: mechanisms and novel therapeutic targets. *Adv Wound Care*. 2018;7(7):209–231. doi:10.1089/wound.2017.0761
51. Kogan S, Sood A, Garnick M. Zinc and wound healing: a review of zinc physiology and clinical applications. *Wounds*. 2017;29(4):102–106.